Journal of Nuclear Materials 384 (2009) 212–221

Contents lists available at ScienceDirect

Journal of Nuclear Materials

journal homepage: www.elsevier.com/locate/jnucmat

Local mechanical properties of Alloy 82/182 dissimilar weld joint between SA508 Gr.1a and F316 SS at RT and 320 °C

Jin Weon Kim [a,*], Kyoungsoo Lee [b], Jong Sung Kim [c], Thak Sang Byun [d]

[a] Department of Nuclear Engineering, Chosun University, 375 Seosuk-dong, Dong-gu, Gwangju 501-759, Republic of Korea
[b] Nuclear Power Laboratory, Korea Electric Power Research Institute, 103-16 Munji-dong, Yusung-gu, Daejon 305-380, Republic of Korea
[c] Department of Mechanical Engineering, Sunchon National University, 413 Jungangno, Sunchon, Jeonnam 540-742, Republic of Korea
[d] Oak Ridge Nation Laboratory, Material Science and Technology Division, P.O. Box 2008, MS-6151, Oak Ridge, TN 37831, United States

ARTICLE INFO

Article history:
Received 20 August 2008
Accepted 13 November 2008

ABSTRACT

The distributions of mechanical and microstructural properties were investigated for the dissimilar metal weld joints between SA508 Gr.1a ferritic steel and F316 austenitic stainless steel with Alloy 82/182 filler metal using small-size tensile specimens. The material properties varied significantly in different zones while those were relatively uniform within each material. In particular, significant gradient of the mechanical properties were observed near the both heat-affected zones (HAZs) of F316 SS and SA508 Gr.1a. Thus, the yield stress (YS) was under-matched with respect to the both HAZs, although, the YS of the weld metal was over-matched with respect to both base metals. The minimum ductility occurred in the HAZ of SA508 Gr.1a at both test temperatures. The plastic instability stress also varied considerably across the weld joints, with minimum values occurring in the SA508 Gr.1a base metal at RT and in the HAZ of F316 SS at 320 °C. The transmission electron micrographs showed that the strengthening in the HAZ of F316 SS was attributed to the strain hardening, induced by a strain mismatch between the weldment and the base metal, which was evidenced by high dislocation density in the HAZ of F316 SS.

1. Introduction

In the primary systems of nuclear power plants (NPPs), the heavy-section low-alloy steel components, such as reactor pressure vessels, steam generators, pressurizer vessels, and large diameter pipelines, are connected to the austenitic stainless steel (SS) pipelines, which require the dissimilar metal weld (DMW) joints between the ferritic and austenitic steels. Alloy 82/182 is commonly used as a filler metal in this type of DMW joint because its thermal expansion coefficient lies between those of ferritic steel and austenitic stainless steel. The alloy also significantly retards the carbon diffusion from the ferritic base metal to the weld metal [1]. Recently, however, a concern has been raised about the integrity of this type of DMW joint because of its high susceptibility to primary water stress corrosion cracking (PWSCC) [2–4]. This has been known to be caused by high residual stress, which is induced by the microstructural heterogeneity and resulting gradient of mechanical properties across the DMW joint. The significant gradient of mechanical properties also produces difficulties in the integrity assessments of the welded components because the stress distribution and crack behavior in the weld joints are strongly dependent on the heterogeneity of mechanical properties [5,6]. Therefore, it is important to further clarify the local distribution of mechanical properties in the weld region for a reliable integrity assessment of the DMW components.

Several studies have attempted to evaluate the local mechanical properties in DMW joints [1,6–10]. Sireesha et al. [1] performed hardness and tensile tests on weldments with Alloys 82 and 182 to select an appropriate filler metal between Alloy 800 and 316LN SS. A series of fracture and tensile tests have also been performed to evaluate the local tensile properties and fracture resistance of DMW joints between SA508 ferritic steel and 304L SS using E308L SS as a filler metal in the BiMET and ADIMEW programs [6–8]. More recently, the tensile properties and local fracture resistance of weld joints between SA508 Gr.3Cl.1 ferritic steel and F316 SS using Alloy 82/182 as a filler metal have been evaluated at room temperature (RT), and the spatial variation of these properties along the width and thickness of the weld joints have been examined [10]. However, they could not obtain reliable tensile data for the Alloy 82/182 fusion area and the heat-affected zone (HAZ) of the SA508 Gr.3Cl.1 because of the size limitations of miniature tensile specimen. Consequently, the local mechanical properties of DMW joints using Alloy 82/182 filler metal have not been properly investigated, despite their importance in determining the reliability of such weldments for many NPP

* Corresponding author. Tel.: +82 62 230 7109; fax: +82 62 232 9218.
E-mail address: jwkim@chosun.ac.kr (J.W. Kim).

0022-3115/$ - see front matter © 2008 Elsevier B.V. All rights reserved.
doi:10.1016/j.jnucmat.2008.11.019

applications. Moreover, there have been no attempts to investigate the mechanical properties of DMW joints using Alloy 82/182 filler metal at NPP operating temperatures.

Therefore, in this study, we obtained the local tensile properties and microstructures of DMW joints using Alloy 82/182 filler metal. A series of tensile tests were performed using small-size flat specimens machined from various material zones of the Alloy 82/182 filler metal joining SA508 Gr.1a ferritic steel and F316 SS. The test results were discussed focusing on the variation of tensile properties such as the yield stress (YS), ultimate tensile strength (UTS), uniform elongation (UE), and plastic instability stress (PIS). It is also attempted to explain these variations in terms of microstructural observations through optical and a transmission electron microscopes (OM and TEM).

2. Materials and experimental procedures

2.1. Tested materials

The weld material used in the experiment was prepared by joining 37 mm thick SA508 Gr.1a ferritic steel and F316 austenitic stainless steel (SS) plates using Alloys 82 and 182 filler wires. SA508 Gr.1a is a low-alloy steel used for main coolant piping and nozzles in nuclear power plants. F316 SS is one of the materials commonly used for branch pipelines and safe-end of nozzles in the primary systems of NPPs. The nominal chemical compositions of both base metals and filler wires are shown in Table 1. Single V-groove welding was adopted for the butt-welding of the plates (Fig. 1). Before groove welding, the SA508 Gr.1a ferritic face was buttered with two layers of Alloy 82 filler metal using manual gas-tungsten arc welding (GTAW), and heat-treated at 610–620 °C for 1.5 h to relieve the residual stresses. Dummy metal blocks were welded at both ends of the base metal plates to provide constraints during the groove welding process, which simulates the conditions in a large structure. In the groove welding, the first 2–3 passes were welded by manual GTAW using Alloy 82 bare wire and additional passes were completed by shielded-metal arc welding (SMAW) using Alloy 182 flux coated filler wire. Fig. 2 presents the welded plate.

Table 1
Nominal chemical composition of base metals and filler wires.

Base metals			Filler metals		
Element	F316	SA508 Gr.1a	Element	Alloy 82	Alloy 182
C	0.08 max.	0.35 max.	C	0.10 max.	0.10 max.
Mn	2.0 max.	0.40–1.05	Mn	2.5–3.5	5.0–9.5
P	0.045 max.	0.025 max.	Fe	3.0 max.	10.0 max.
S	0.03 max.	0.025 max.	P	0.03 max.	0.030 max.
Si	1.0 max.	0.15–0.40	S	0.015 max.	0.015 max.
Ni	11.0–14.0	0.40 max.	Si	0.50 max.	1.0 max.
Cr	16.0–18.0	0.25 max.	Cu	0.50 max.	0.50 max.
Mo	2.0–3.0	0.10 max.	Cr	18.0–22.0	13.0–17.0
V	–	0.05 max.	Ti	0.75 max.	1.0 max.
Cu	–	–	Nb + Ta	2.0–3.0	1.0–2.5
Al	–	–	Ni + Co	67.0 min.	59.0 min.
Fe	Balance	Balance	Other	0.50 max.	0.50 max.

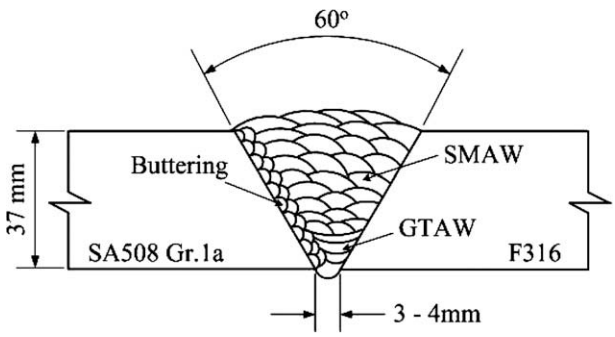

Fig. 1. Schematic diagram of the dissimilar metal weld design and welding procedure.

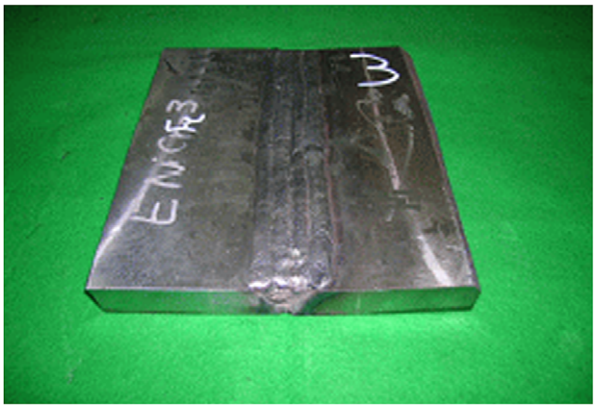

Fig. 2. Photograph of an as-welded plate.

2.2. Specimens and tensile tests

Two types of tensile specimens were employed: small-size flat specimen with cross-section of 0.5 mm × 2.0 mm and uniform length of 14.0 mm; and standard cylindrical specimens, 4.0 mm in diameter and 30.0 mm in uniform length (Fig. 3). The small-size flat specimens were used to measure the local tensile properties, while the standard cylindrical specimens were used to confirm the reliability of the data obtained from the small-size flat specimens. The dimensions of small-size specimen were determined from the widths of HAZs and buttering layers measured macroscopically. The welded plates were first cut into six blocks: four blocks for the small-size flat specimens and two blocks for the standard cylindrical specimens. Specimens were extracted from each block using electro-discharge machining (EDM) (Fig. 4). Regardless of the type, all specimens were machined along the

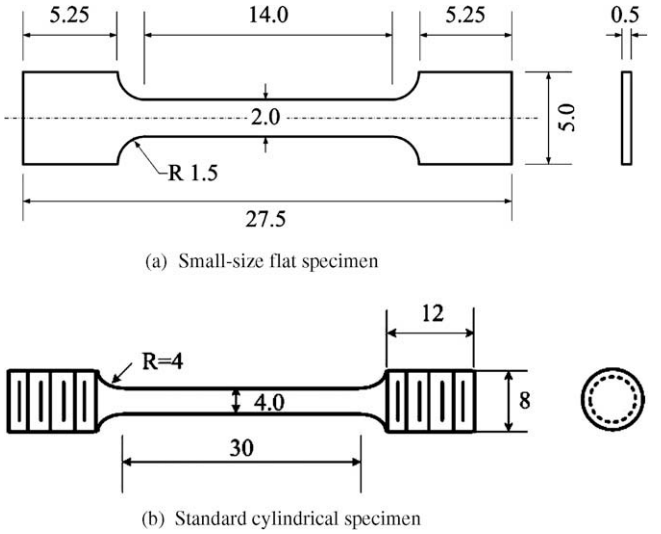

Fig. 3. Dimensions of the tensile specimens (the scale in mm).

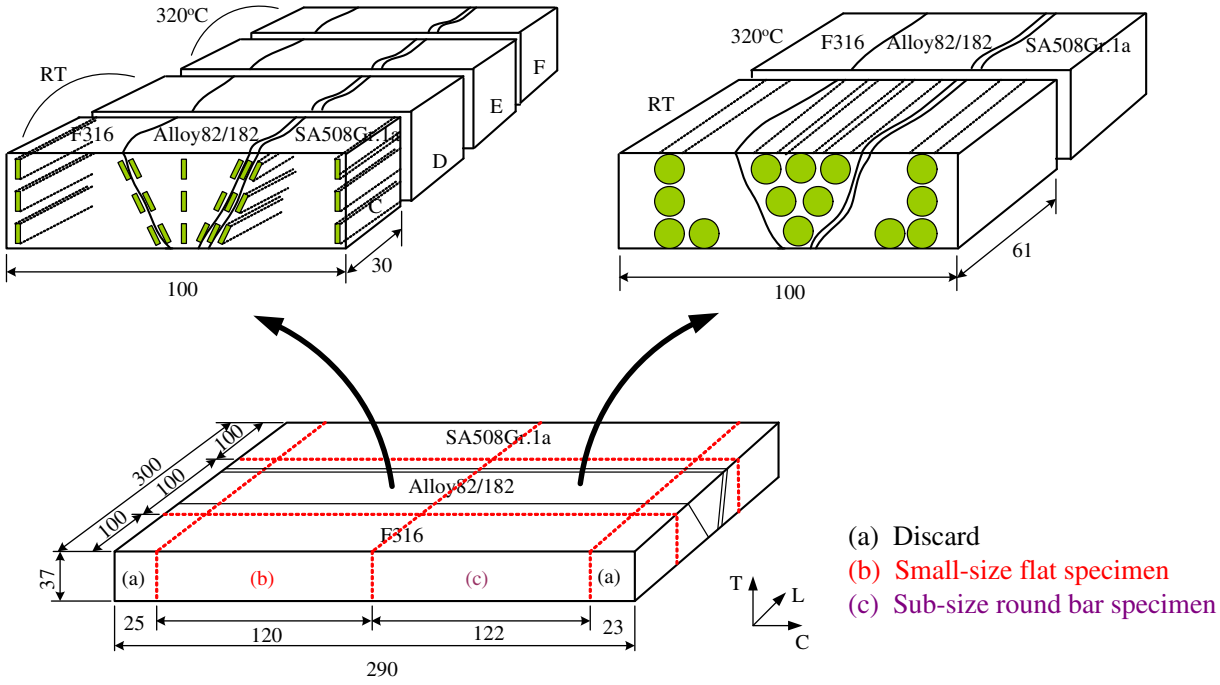

Fig. 4. Schematic descriptions of the specimen extraction from the weld joint.

direction of the weldment, i.e., parallel to the fusion line. Small-size flat specimens were taken from different material zones across the weld joint, including the weld metal, buttering layer, ferritic and austenitic HAZs, and both base metals at three different thickness locations: at the bottom, mid-point, and top of weld. For the weld metal, the specimens were also taken from both boundaries near the fusion line as well as the center of the weld to examine the variations of tensile properties within the Alloy 82/182 fusion area (Fig. 5). The standard cylindrical specimens were taken from three typical material zones covering both base metals and the Alloy 82/182 fusion area.

Tensile tests were conducted using a motor-driven universal testing machine at RT and 320 °C in air at a nominal strain rate of 5×10^{-4}/s. Displacement was measured using extensometers with gage lengths of either 10 mm or 25 mm, depending on the specimen type. Fig. 6 shows small-size flat specimens and a testing setup at RT.

2.3. Examination of microstructures

The cross-sections were polished and etched to clarify the different material zones in the weldment cross-sections and to examine the microstructure of each material zone. Different solutions were used depending on the material zone to ensure proper etching: a 3% natal solution for SA508 Gr.1a base metal and its HAZ, Kalling's reagent for F316 SS base metal and its HAZ, and electrolytic etching for the Alloy 82/182 fusion area and buttering layer [11]. The microstructures in each material zone were observed using an optical microscope (Olympus model GX51). Additionally, the transmission electron microscopy was performed in a JEOL JEM-2100F at 200 kV to examine the metallurgical characteristics of F316 SS and its HAZ.

3. Results and discussion

3.1. Microstructures

The weld cross-section was identified by etching as the base metals, Alloy 82/182 fusion area, buttering layer, and HAZ of SA508 Gr.1a, but HAZ of F316 SS side was not identified macroscopically. Fig. 7 shows the optical microstructures of all material zones identified. The SA508 Gr.1a and F316 SS base metals exhibited typical tempered bainite and equiaxed austenitic grains with delta ferrite in the form of stringers, respectively. The Alloy 82/

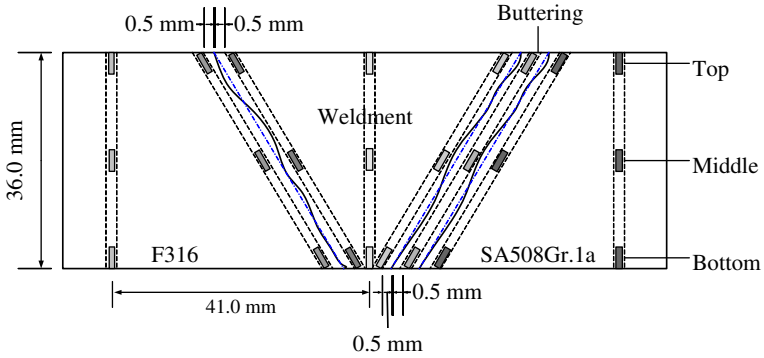

Fig. 5. Locations of the small-size flat specimens at the dissimilar metal weld joint.

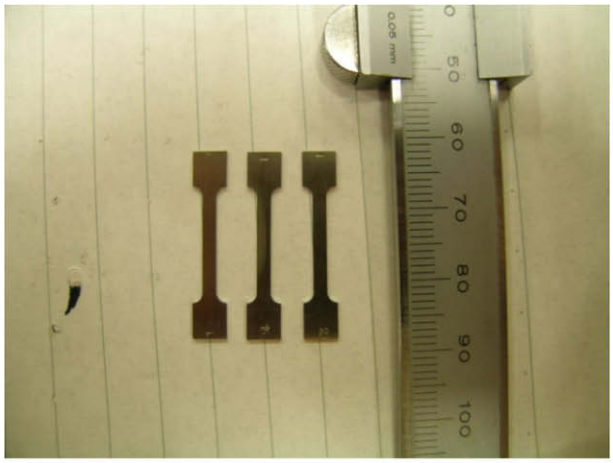

(a) Small-size flat specimens (the scale in mm)

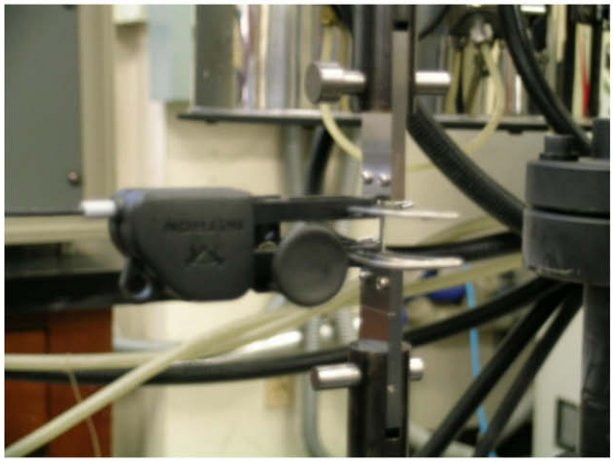

(b) Test set-up

Fig. 6. Photographs of the small-size flat specimens and the test set-up.

182 fusion areas were fully austenitic with typical dendritic structures developed along the direction of cooling and recrystallized features with extensive grain boundary migration resulting in large grains >200 μm. The Alloy 82/182 buttering layer had microstructure similar to that of the Alloy 82/182 fusion area, consistent with previous studies [1,10,12]. It is known that the driving force of the migration is the same as simple grain growth in base metals [13]. The SA508 Gr.1a ferritic steel adjacent to the buttering layer had distinguishable microstructures from those of the SA508 Gr.1a base metal, characterized by a HAZ with a specific microstructural width of ~1.5 mm. It is known that the microstructures of the ferritic HAZ depend on their distance from the fusion line, and various microstructures have developed within such regions by phase transformation [6]. The present observations also revealed a carbon depletion area, coarse-grained upper bainitic area, and small ferrite/bainite grained area from the fusion line to the base metal. No specific microstructures were observed near the fusion line on the F316 SS side of the weld joint.

3.2. Stress–strain behavior

The true stress–true strain curves obtained from the different material zones of the DMW joint using the small-size flat specimens were compared at RT and 320 °C (Fig. 8). The curves were calculated from the engineering stress–strain data in the uniform elongation range. The stress–strain curves exhibited the same pattern with relatively little variation within the same material zone, except for the HAZ of SA508 Gr.1a which shows significant variation. However, the curves exhibited different patterns between the different material zones across the DMW joint at both test temperatures.

Within the Alloy 82/182 fusion area, the difference in the stress–strain curves for the center and boundaries of the weldment were small, but the variation through the thickness were pronounced and consistent, particularly at the center of the fusion area where the stress–strain curve at the bottom (root) was higher than that at the top of the weldment at both temperatures. The strength differences between the top and bottom of welds have also been observed in prior DMW joint studies [6,7,10], but the causes of those differences have not been clearly explained. It is assumed that such strength differences are not related to the type of filler metal or the shape of the welded components because they have also been observed in DMW joints between pipes using 308L austenite SS as the filler metal [6,7]. The stress–strain behavior of the Alloy 82/182 buttering layer and fusion area was also similar at both temperatures, which is consistent with similar microstructures in both regions.

Both ferritic and austenitic HAZs showed substantially higher stress–strain curves and different hardening behaviors compared to their base metals. Considerable scatter was seen in the stress–strain behavior for the ferritic HAZ of SA508 Gr.1a at both test temperatures. Stress fluctuations, i.e., serrations, were observed in the stress–strain curves tested at 320 °C for both base metals and their HAZs, which indicates dynamic strain aging (DSA) occurs at that temperature [14,15].

3.3. Spatial variation of tensile properties

A comparison of the true stress–true strain curves indicates that the tensile properties have relatively little variation within the same material zone, but display considerable variation between different material zones across the DMW joint. Thus, the local tensile property parameters, such as the YS, UTS, UE, and PIS, were evaluated from the tensile test results for the small-size flat specimens, and their variations across the weld joint were investigated at both room and NPP operating temperatures.

3.3.1. Validation of tensile data

Prior to examining the local tensile properties measured at each material zone, the tensile data were compared with the results from the standard cylindrical specimens to confirm the validity of the data from the small-size flat specimens. Table 2 summarizes the data from both specimens for the base metals and Alloy 82/182 filler metal at RT and 320 °C. No significant differences were observed except for the significantly lower elongations of Alloy 82/182 weld metal from the small-size flat specimens; the differences were less than 20% for other cases. This result confirms that the local tensile properties measured from the small-size flat specimens are reliable.

Typically, the specimen thickness should be >4–6 times the grain size to obtain reliable material tensile properties [16]. Considering the grain size of the Alloy 82/182 weld metal, which was greater than 200 μm, the thickness of our small-size flat specimens was less than this requirement. A prior study used miniature specimens with cross-sections of 0.28 mm × 1.2 mm showed a considerable underestimation of the UTS for the Alloy 82/182 weld metal, which was known to be associated with the unsatisfying thickness requirement [10]. However, the present results show that small-size flat specimens of thickness >0.5 mm can still provide reliable tensile properties, even though they do not satisfy the typical thickness requirement.

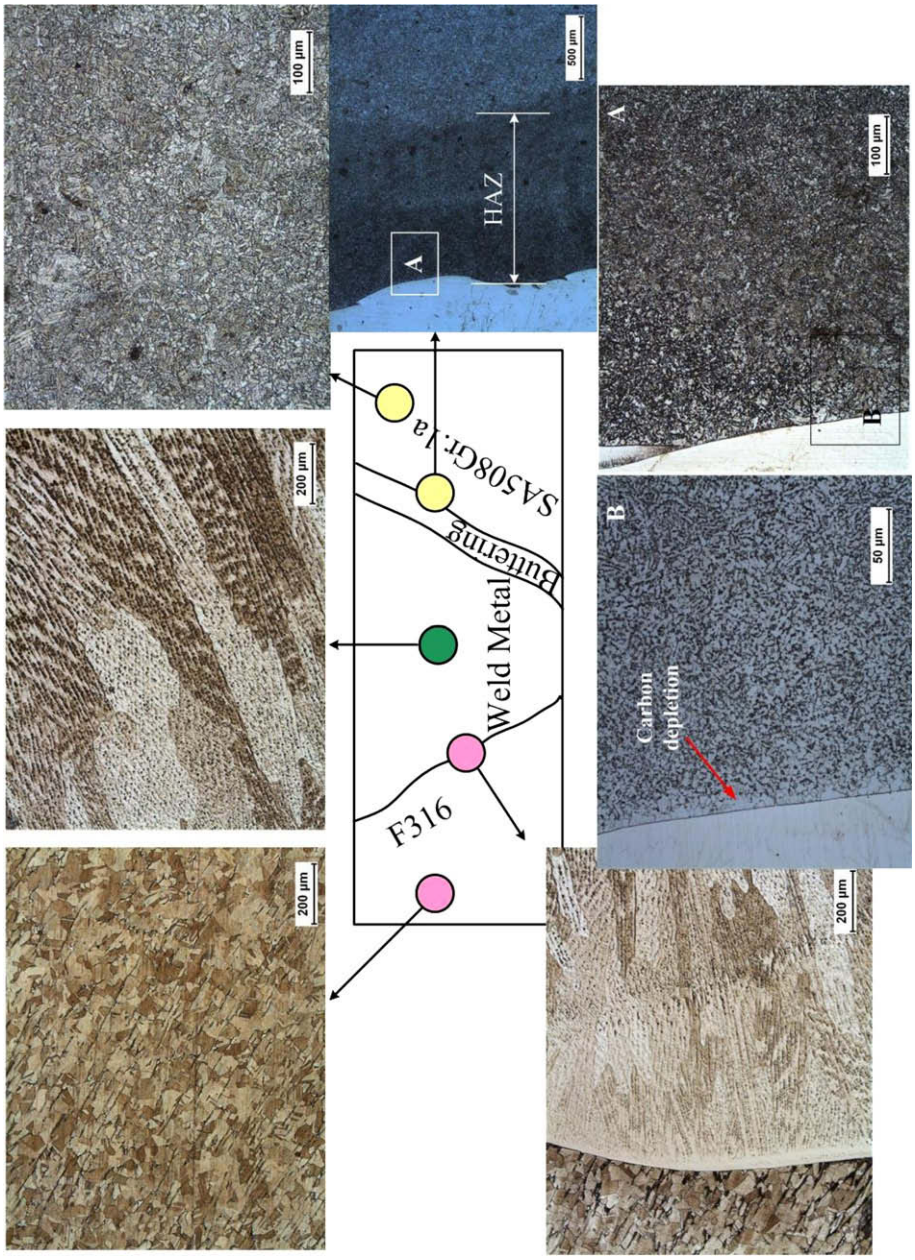

Fig. 7. Microstructures of different material zones of the Alloy 82/182 dissimilar metal weld joint between SA508 Gr.1a and F316 SS plates.

3.3.2. Yield stress and ultimate tensile stress

Fig. 9 presents the spatial variations of the YS and UTS across the weld joint. It is shown that the variations in YS were similar at both RT and 320 °C, even though the YS values at 320 °C were lower than those at RT in all material zones. Regardless of the different test temperatures, the average YS values of the Alloy 82/182 weld metal were greater than those of the two base metals, and the variation of the YS within the Alloy 82/182 fusion area was insignificant (<10%). The YS in the buttering layer behaved similarly to that of the adjacent weld metal; however, the YS drastically increased and peaked in the HAZs of SA508 Gr.1a and F316 SS. The YS values in both HAZs were not only about 50% higher than those of respective base metals but also about 30% higher than those of the adjacent Alloy 82/182 weld metal and buttering layer. Thus, a significant YS gradient occurred near the HAZs at both RT and 320 °C (Fig. 9(a)).

The spatial variation of the UTS exhibited a different trend with test temperature, as shown in Fig. 9(b). At RT, the variation of the UTS across the weld joint was insignificant, less than several percent, except for the SA508 Gr.1a base metal, which had a lower UTS value compared to other material zones. However, at 320 °C, the variation of the UTS across the weld joint was considerable. The Alloy 82/182 fusion area and buttering layer had substantially lower UTS values than that of the adjacent HAZ of SA508 Gr.1a, while the UTS value in the weld boundary was about 90 MPa higher than that in the adjacent HAZ of F316 SS. This was because the temperature dependence of the UTS differed with the material zone. The UTS of the SA508 Gr.1a base metal and its HAZ slightly increased at 320 °C compared to RT due to the occurrence of DSA, as indicated by the serration in the stress–strain curves, while for other material zones, the UTS decreased with increasing temperature. The reduction of UTS was especially significant for F316

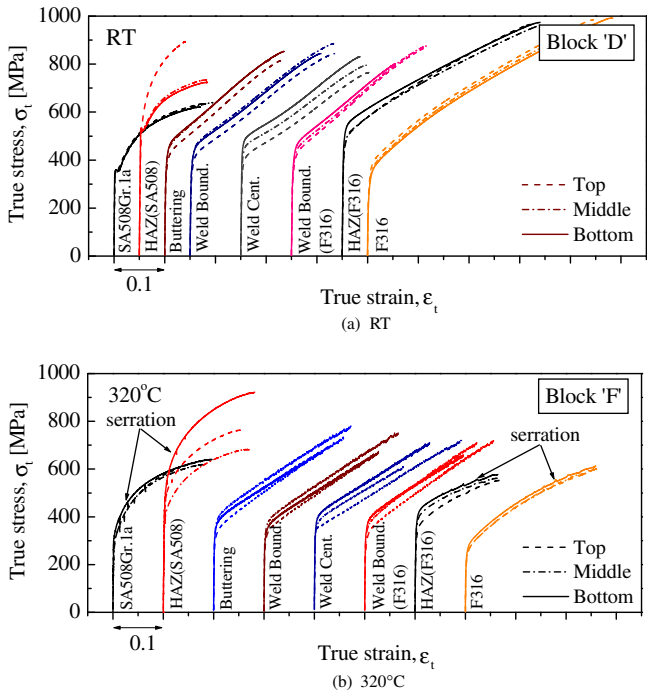

Fig. 8. Comparison of the true stress–strain curves obtained from each material zone of the dissimilar metal weld joint between SA508 Gr.1a and F316 SS with Alloy 82/182 filler metal.

SS and its HAZ; the minimum value was observed in the F316 SS base metal. Within the Alloy 82/182 fusion area, the UTS of the weld center was lower than that of the weld boundaries at both test temperatures, but the difference was <10%.

In the welded components, the weld strength mismatch with base metal is important because it has a strong influence on the crack driving force and crack growth. The yield stress ratio has been used as an indicator of the strength mismatch, expressed as:

$$\text{Yield stress ratio, } M = YS_{WM}/YS_{BM}, \quad (1)$$

where YS_{WM} and YS_{BM} are the yield stresses of the weld metal and base metal, respectively. If the welds under-match ($M < 1$), a strain concentration will occur in the weld metal and fracture initiation can occur from pre-existing defects. Therefore, it is important to achieve a strength over-matching ($M > 1$) weld design to ensure strong weld joints [5,6]. We calculated the weld strength mismatch ratio using the average YS value at each material zone of the DMW joint to quantitatively investigate the effect of the spatial variation in YS on the integrity assessment of the weld joint. The YS mismatch ratios are summarized in Table 3. At both test temperatures, the Alloy 82/182 weld was over-matched with respect to both base metals by 1.13–1.43, but the buttering layer and weld boundary were under-matched with respect to both HAZs by 0.78–0.92. Regardless of the test temperature, the highest over-match ratio occurred between the Alloy 82/182 weldment and the F316 SS base metal; the under-match was the most significant between the buttering layer and HAZ of SA508 Gr.1a. Generally, the effect of a mismatch is considered significant when the strength of mismatched materials exceeds 10% [5]. Therefore, the strength mismatching effect should be taken into account during the integrity assessment of DMW joints between SA508 Gr.1a ferritic steel and F316 SS with Alloy 82/182 filler metal. These results also indicate that plastic strain concentration and fracture initiation do not occur at the Alloy 82/182 fusion area, but rather at the F316 SS base metal and between the buttering and HAZ at both temperatures. With respect to crack prop-

Table 2
Comparisons of tensile properties tested using standard and small-size flat specimens.

Test temperature	Materials	Yield stress, YS [MPa]			Ultimate tensile stress, UTS [MPa]			Uniform elongation, UE [%]			Total elongation, TE [%]		
		Standard specimen	Small-size flat specimen	Difference [%]	Standard specimen	Small-size flat specimen	Difference [%]	Standard specimen	Small-size flat specimen	Difference [%]	Standard specimen	Small-size flat specimen	Difference [%]
RT	SA508Gr.1a	345.0 ± 11.1	343.6 ± 7.0		515.4 ± 0.8	522.1 ± 2.9	1.30	15.7 ± 0.2	15.9 ± 0.6	1.27	28.2 ± 0.5	25.9 ± 1.7	−8.2
	Alloy 82/182	387.6 ± 15.0	413.2 ± 38.4	6.60	637.3 ± 11.1	621.6 ± 28.9	−2.46	33.1 ± 2.4	27.8 ± 1.6	−16.01	37.4 ± 3.0	30.9 ± 1.8	−17.4
	F316 SS	298.3 ± 6.0	305.2 ± 13.1	2.31	599.4 ± 2.01	624.4 ± 6.3	4.17	52.1 ± 0.9	53.7 ± 1.7	3.07	66.0 ± 2.3	61.5 ± 3.0	−6.8
320 °C	SA508Gr.1a	275.3 ± 1.2	288.0 ± 8.8		514.7 ± 1.7	530.2 ± 7.8		14.4 ± 0.8	16.7 ± 0.8	15.97	24.1 ± 0.4	24.9 ± 1.8	3.3
	Alloy 82/182	315.8 ± 16.2	347.8 ± 37.8	10.1	542.7 ± 13.8	526.9 ± 21.4	−2.91	33.0 ± 3.1	26.2 ± 4.7	−20.6	36.4 ± 2.5	26.7 ± 5.7	−26.6
	F316 SS	199.8 ± 8.8	232.2 ± 10.6	16.2	439.6 ± 1.4	463.7 ± 4.8	5.48	26.9 ± 0.2	28.4 ± 1.1	5.58	32.5 ± 0.0	31.9 ± 2.6	−1.8

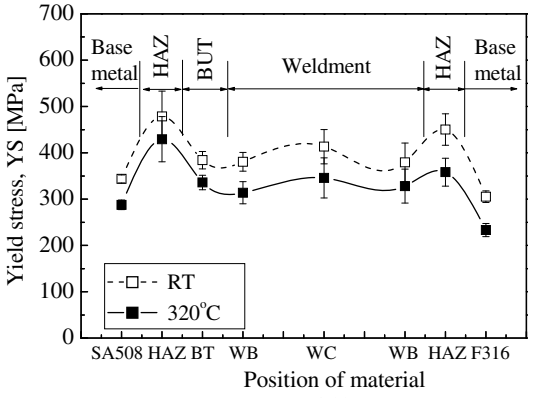

(a) Yield stress

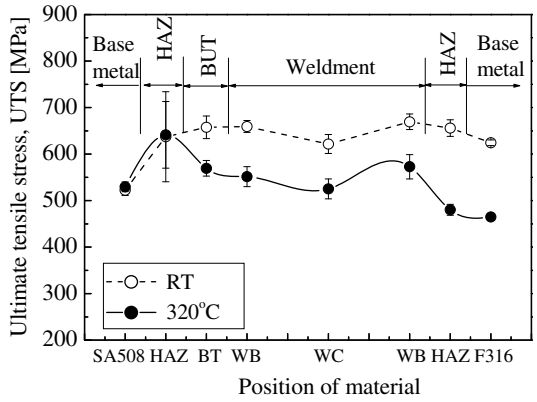

(b) Ultimate tensile stress

Fig. 9. Spatial variations of the yield stress and ultimate tensile stress across the weld joint between SA508 Gr.1a and F316 SS with Alloy 82/182 filler metal at RT and 320 °C.

Table 3
Comparisons of strength mismatch ratios, *M*, at RT and 320 °C.

Location		RT	320 °C
Ferritic side	Weldment vs. SA508 Gr.1a, $M_{WM\text{-}SA508}$	1.13372	1.15072
	Buttering vs. HAZ, $M_{BU\text{-}HAZ}$	0.80246	0.78247
Austenitic side	Weldment vs. F316, $M_{WM\text{-}F316}$	1.27533	1.42797
	Weld boundary vs. HAZ, $M_{WB\text{-}HAZ}$	0.84255	0.91605

agation, the interface between the buttering layer and the HAZ of SA508 Gr.1a, where *M* was the lowest, indicated a critical location in this weld joint because the higher the strength mismatch ratio between interfacial materials, the higher the interfacial crack tip stresses.

3.3.3. Ductility

The UE values were evaluated at each material zone over the weld cross-section to investigate the variation of ductility across the DMW joint. Fig. 10 presents the UEs at RT and 320 °C as functions of the position. The UE was almost constant within the Alloy 82/182 fusion area and buttering layer at both test temperatures. Also, the temperature dependence of UE was negligible in this material zone. Both SA508 Gr.1a and F316 SS HAZs showed lower elongations than their base metals, and the minimum UE across the weld joint always appeared at the HAZ of SA508 Gr.1a at both test temperatures. The UE in the F316 SS base metal and its HAZ were dramatically reduced at the higher test temperature. The ductility in the HAZ of F316 SS was lower than that in the Alloy

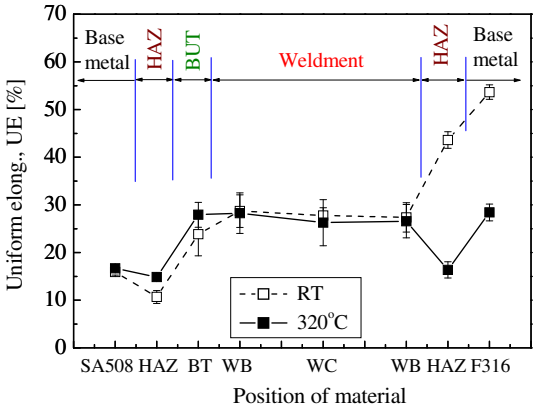

Fig. 10. Spatial variations of the uniform elongation across the weld joint between SA508 Gr.1a and F316 SS with Alloy 82/182 filler metal at RT and 320 °C.

82/182 fusion area and comparable to that of the ferritic side HAZ. The loss of ductility in 316 SS near the operating temperature of NPPs has been observed in other studies; this has been explained by a mechanism involving the disappearance of twinning-induced hardening [17] and by the occurrence of DSA [15]. However, the mechanism of loss of ductility in the NPP operating temperature range is still unclear.

3.3.4. Plastic instability stress

As discussed in the previous section, the YS ratio between the weld metal and surrounding materials is an important parameter that represents the strength mismatch of a weld, which governs the location of the strain concentration in the weld joint and affects crack driving force under fully plastic conditions. However, the values of the UTS and UE, which are material properties related to the deformation and ductile failure of hardening material, also varied considerably across the DMW joint at NPP operating temperatures, and their patterns were different from that of the YS. Therefore, we investigated the variation of the PIS across the weld joint. The PIS is defined by the true stress at onset of necking or is a true stress version of UTS; it can reflect variations in the UTS and UE as follows:

$$\mathrm{PIS} = \mathrm{UTS} \times (\mathrm{UE}[\%]/100 + 1). \quad (2)$$

Since the PIS is strongly dependent on temperature but independent of the stress concentration and irradiation dose levels [17–19], its value is an inherent material property that represents the resistance of the local necking initiation [18]. It is also commonly used as a local failure criterion for ductile material [19].

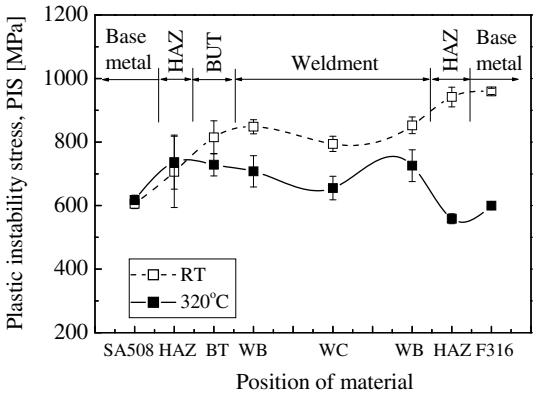

Fig. 11. Spatial variations of the plastic instability stress across the weld joint between SA508 Gr.1a and F316 SS with Alloy 82/182 filler metal at RT and 320 °C.

The PIS varied across the weld joint (Fig. 11). At RT, the lowest PIS appeared in the SA508 Gr.1a base metal while the highest PIS appeared on the other side in the F316 SS base metal. At NPP operating temperatures, however, the PISs of F316 SS and its HAZ were substantially lower than those of the other material zones; the minimum occurred in the HAZ of F316 SS. At both test temperatures, the Alloy 82/182 fusion area always showed an intermediate PIS value. Therefore, at RT, necking in the DMW joint occurs in the SA508 Gr.1a base metal after the plastic deformation initially occurs in the F316 SS base metal, which has the lowest YS. At NPP operating temperatures, the plastic strain initially occurs in the F316 base metal, but necking is generated in the HAZ of F316 SS after deformation. Although the locations of necking and final failure do not always correspond, this result indicates that the possibility of ductile failure induced by necking deformation in the Alloy 82/182 weldment and buttering layer is very low in the weld joint between SA508 Gr.1a and F316 SS, regardless of the temperature.

3.4. Characteristics of the HAZs

As discussed in the previous sections, the YS peaked in the HAZs of F316 SS and SA508 Gr.1a. The UTS gradients were also considerable in these HAZs at 320 °C. Furthermore, there was a considerable scattering in the YS and UTS values for the HAZ of SA508 Gr.1a. Therefore, additional tensile tests were conducted using small-size flat specimens at RT to obtain higher resolution data and better understand the characteristics of these HAZs. All specimens were machined along the weld direction from the material region near the fusion line to 5 mm from the fusion line (Fig. 12). The YS and UTS values are presented as a function of distance from the fusion line in Fig. 13. A significant gradient of in the YS and UTS values was observed in the HAZ of SA508 Gr.1a within the material region considered (Fig. 13(a)). The YS and UTS values peaked at distance of about 1 mm from the fusion line rather than at a point closer to the fusion line. The peak YS and UTS values were 60% and 35% higher than those of the SA508 Gr.1a base metal, respectively. Both the YS and UTS values decreased dramatically beyond 1 mm from the fusion line and then saturated, however, even the saturated YS value was higher than that of the SA508 Gr.1a base metal. A significant increase in strength occurred in the narrow material zone 1 mm from the fusion line, even though the material within 5 mm from the fusion line was affected by welding. Comparing with the microstructures observed in the HAZ of SA508 Gr.1a, it is clear that the narrow material zone corresponding to the peak values of YS and UTS coincided with the coarse-grained upper bainitic zone, while the region with the saturated YS coincided with the small grained ferritic/bainitic zones. We speculate that the lower YS and UTS values in the region immediately adjacent to the fusion line relative to the region 1 mm from the fusion line are associated with the carbon depletion generated during the post-weld heat treatment after buttering. These microstructural variations within the HAZ might also have caused the scattering

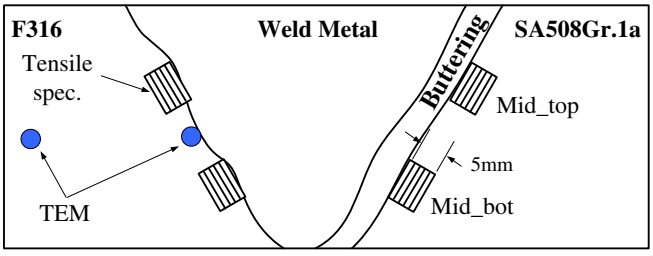

Fig. 12. Locations of the small-size flat specimens and TEM specimens near the fusion line for characterizing the properties of heat-affected zones.

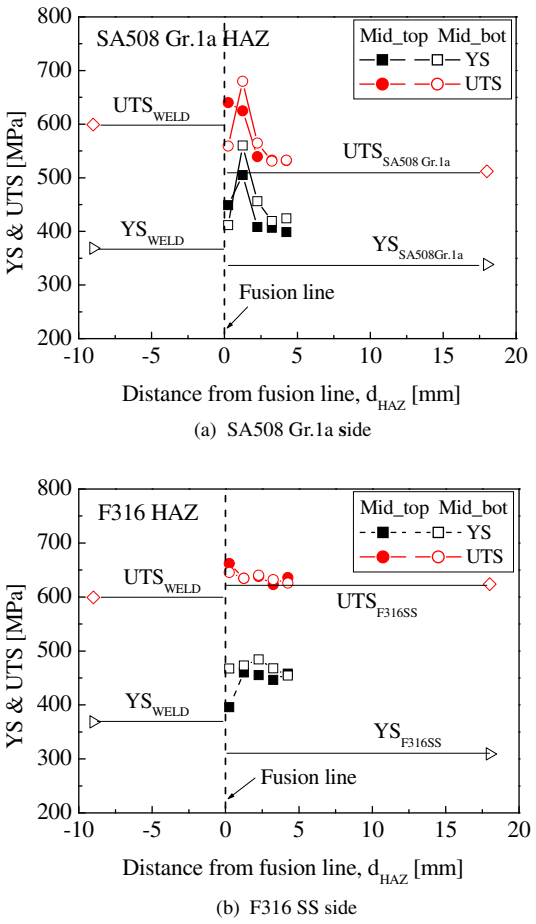

Fig. 13. Variations in the yield stress and ultimate tensile stress within the heat-affected areas of SA508 Gr.1a and F316 SS.

of the tensile properties. Consequently, the specific characteristics of the HAZ of SA508 Gr.1a can be attributed to the different microstructures within the HAZ developed by the phase transformation during the welding process.

In the HAZ of F316 SS, the YS was about 50% higher than that in F316 SS base metal, while the UTS increment was <8% (Fig. 13(b)). Compared to the HAZ of SA508 Gr.1a, the variations in the YS and UTS were insignificant in this material region. Therefore, the welding effect was more pronounced in the YS rather than the UTS, while the hardening mechanism was almost identical within the entire heat-affected region. In contrast, the hardening mechanism for F316 SS was not obvious because the microstructures of F316 SS were not changed by the temperature fluctuation that occurred during the welding process. Most previous DMW joint studies have expressed little concern about mechanical property changes in the HAZs of austenitic SSs, and only a few studies observed hardening in the HAZ of SS [1,9,10] that can be attributed to grain recrystallization and carbide precipitation [10]. However, these attributions are insufficient to explain the characteristics of the HAZ of F316 SS. Therefore, we investigated the microstructures of the F316 SS base metal and its HAZ further using a TEM (Fig. 12).

As shown in Fig. 14 the micrographs of F316 SS base metal demonstrated that no excessive carbide precipitation was present in its HAZ, whereas the dislocation density was substantially higher in the austenitic HAZ than in the F316 SS base metal. This indicates that the strength increase in the HAZ of F316 SS was primarily caused by strain hardening rather than by carbide precipitation; which agrees with the observations presented in the previous

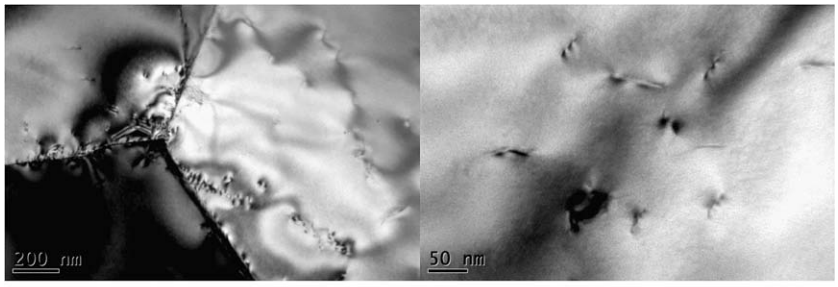

(a) F316 base metal

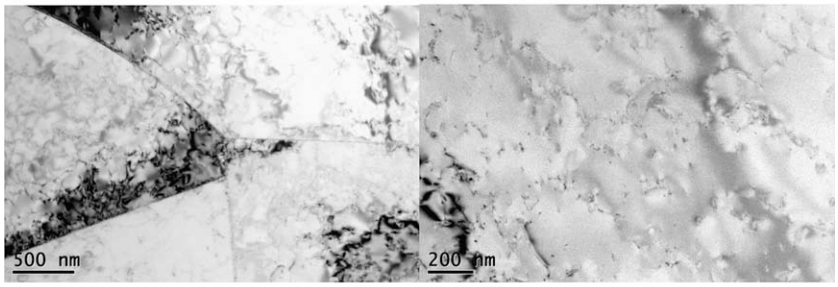

(b) F316 HAZ

Fig. 14. Comparison of TEM micrographs observed from the base metal and the heat-affected zone of F316 SS.

section, namely, that the heat effect was dominant at YS, the UTS of HAZ area substantially decreased with increasing test temperature, and the PIS in the HAZ was almost identical to that of the F316 SS base metal. In general, cold work increases the YS of materials under remaining work hardening rates [20,21], and the hardening rates of cold-worked materials substantially decrease with increasing test temperatures [21]. Also, the PIS is nearly independent of prior cold work [21]. The strain hardening in the HAZ of F316 SS is attributed to the successive heating and cooling that take place in this material region during the welding process, introducing stain mismatching between weldment and base metal which causes residual stress [22]. Since the thermal expansion coefficient of F316 SS is particularly high, the strain mismatch is a dominant at the interface between weldment and F316 SS.

4. Conclusions

The tensile property distributions in dissimilar metal weld joints between SA508 Gr.1a and F316 SS using an Alloy 82/182 filler metal were evaluated using small-size flat specimens at both room temperature and a typical nuclear power plant operating temperature (320 °C). In addition, the microstructures of the materials were examined using optical and transmission electron microscopy to characterize the different material zones across the width and thickness of the DMW joint. The following conclusions can be drawn from the results.

(1) Small-size flat specimens with cross-sections of 0.5 mm × 2.0 mm provided reliable local tensile properties for the various material zones in the DMW joint, including the large-grained Alloy 82/182 weldment.
(2) The stress–strain curves exhibited relatively little variation within the same material zone, but considerable variation between different material zones over the weld joint. Within the Alloy 82/182 fusion area, the difference in the stress–strain curves between the weld center and boundaries was minimal, whereas the difference along the thickness of the weld was more obvious. The bottom (root) of the weld exhibited higher stress–strain curves than the top of weld at both RT and 320 °C.
(3) The YS of the Alloy 82/182 weld metal was over-matched with respect to both base metals by 1.13–1.43, but undermatched with respect to both HAZs, including the HAZ of F316 SS, where the YS peaked, by 0.78–0.92. The undermatch was most significant at the interface between the buttering layer and the HAZ of SA508 Gr.1a at 320 °C.
(4) The spatial variation of UTS across the weld joint was insignificant at RT. However, at 320 °C, the variation was significant at the interface between the HAZ of SA508 Gr.1a and the buttering layer and also between the Alloy 82/182 weld boundary and the HAZ of F316 SS.
(5) At both test temperatures, the minimum ductility in the DMW joint occurred in the HAZ of SA508 Gr.1a. The ductility of F316 SS base metal and its HAZ were dramatically reduced at the higher temperature, and thus the ductility in the HAZ of F316 SS was comparable with that in the HAZ of SA508 Gr.1a at 320 °C.
(6) The PIS also considerably varied across the weld joint. The minimum values appeared in the SA508 Gr.1a base metal at RT and in the HAZ of F316 SS at 320 °C. Therefore, the possibility of ductile failure by necking deformation at the Alloy 82/182 weldment, including the buttering layer, is very low at both temperatures.
(7) Significant gradients of the YS and UTS were observed within the HAZ of SA508 Gr.1a. This was attributed to the different microstructures within the HAZ resulting from the phase transformation during welding. However, the welding effect dominated the YS rather than UTS in the HAZ of F316 SS, and TEM micrographs conformed the strengthening in the HAZ of F316 SS was associated with a dislocation-induced strain hardening.

Acknowledgements

The authors express special thanks to Drs T.L. Sham and W.C. Woo for their technical reviews and thoughtful comments.

References

[1] M. Sireesha, S.K. Albert, V. Shankar, S. Sundaresan, J. Nucl. Mater. 279 (2000) 65.

[2] J.I. Bennetch, G.E. Modzelewski, L.L. Spain, G.V. Rao, in: P.S. Lam (Ed.), Service Experience and Failure Assessment Applications ASME 2002, ASME PVP, vol. 437, New York, 2002, pp. 179–185.
[3] USNRC, Information Notice 2000-17, Crack in Weld Area of Reactor Coolant System Hot Leg Piping at V.C. Summer, 18 October 2000.
[4] USNRC, Information Notice 2002-11, Recent Experience with Degradation of Reactor Pressure Vessel Head, 12 March 2002.
[5] D.S.R. Murthy, IE (I) Journal-CV 84 (2003) 136.
[6] A. Laukkanen, P. Nevasmaa, U. Ehrnsten, R. Rintamaa, Nucl. Eng. Des. 237 (2007) 1.
[7] K-H. Schwalbe, A. Cornec, D. Lidbury, Int. J. Pres. Ves. Pip. 81 (2004) 251.
[8] N. Taylor, C. Faidy, P. Gilles, Assessment of Dissimilar Weld Integrity: Final Report of the NESC-III, EUR 22510 EN, 2006.
[9] A. Celik, A. Alsaran, Mater. Charact. 43 (1999) 311.
[10] C. Jang, J. Lee, J.S. Kim, T.E. Jin, Int. J. Pres. Ves. Pip. 85 (2008) 635.
[11] F. George, V. Vander, ASM Handbook, vol. 9, ASM, 2004.
[12] R. Dehmolaei, M. Shamanian, A. Kermanpur, Mater. Charact. (in press) doi:10.1016/j.matchar.2008.01.013.
[13] J.C. Lippold, D.J. Koteki, Welding Metallurgy and Weldability of Stainless Steels, John Wiley, 2005.
[14] I.S. Kim, S.S. Kang, Int. J. Pres. Ves. Pip. 62 (1995) 123.
[15] S.G. Hong, S.B. Lee, J. Nucl. Mater. 340 (2005) 307.
[16] N. Igata, K. Miyahara, T. Uda, S. Asada, in: W.R. Corwin, G.E. Lucas (Eds.), The Use of Small-Scale Specimens for Testing Irradiated Material, ASTM STP 888, ASTM Philadelpia, 1986.
[17] X. Wu, X. Pan, J.C. Mabon, M. Li, J.F. Stubbins, J. Nucl. Mater. 356 (2006) 70.
[18] T.S. Byun, K. Farrell, Acta Mater. 52 (2004) 1597.
[19] J.W. Kim, D.H. Kim, C.Y. Park, S.H. Lee, Tans. KSME 31 (2007) 304.
[20] W.D. Callister Jr., Materials Science and Engineering: An Introduction, 6th Ed., John Wiley, 2003.
[21] T.S. Byun, N. Hashimoto, K. Farrell, Acta Mater. 52 (2004) 3889.
[22] R. Stoenescu, R. Schaeublin, D. Gavillet, N. Baluc, J. Nucl. Mater. 362 (2007) 287.